Chapter 6

CB-like Microstructure in a CoFeGaMnZn Multicomponent Oxide (MCO)

6.1 Introduction

In this chapter, we have endeavoured to design a new material with CB-like microstructure in the light of understanding of the detailed investigations that have been covered in the previous chapters. The thought behind developing a new CB-like system is to design a material that can emanate exotic functional properties. In this thesis, Chapter 3, Chapter 4 and Chapter 5 comprise CB-like microstructural evolution in spinel and perovskite systems. Mn-doped $CoFe_2O_4$ and $ZnGa_2O_4$ have been covered in spinel systems, while $LiNdTiO_3$ system has been studied in perovskite system. CB-like nanostructure in Mn-doped $CoFe_2O_4$, is found to be an interlacing of two distinct $CoMn_2O_4$ (paramagnetic), $CoFe_2O_4$ (ferrimagnetic) domains [1]. In this case the evolution of the CB-like microstructure happens through an interpenetration of twinned domains evolved with a recurrent phase separation followed by concatenation of cuboidal/octahedral nanodomains along <004> directions. In the same line, Mn-doped $ZnGa_2O_4$ system also evolves with $ZnGa_2O_4$ and $ZnMn_2O_4$ nanodomains self-assembled into well-organized CB-like microstructure. In Mn-doped $CoFe_2O_4$ microstructure, constituent nanodomains have been reported as magnetically anisotropic with high coercivity, which can be utilized to develop materials for perpendicular magnetic storage devices [2]. In the same line, we have attempted to develop a CB-like microstructure consisting of two or more well-organized ferrimagnetic nanodomains with different magnetic strengths instead of a periodic interlacing of paramagnetic and ferrimagnetic nanodomains so that it can be utilized for the same application but with improved areal density ($TB/inch^2$) and archivability [3]. New system is also expected to circumvent the trilemma of any magnetic memory storage device (explained in Chapter 1). To fulfil this demand, we propose a multicomponent oxide (MCO) system based on elements, i.e., Fe, Co, Zn, Ga in the authority of Mn^{+3} that can be evolved as CB-like microstructure. Mn^{+3} is used to exploit its exceptional ability to introduce high J-T distortion (>10%) in the spinel structure [4]. In spinel systems, Mn^{+3} ion becomes J-T active once it occupies the octahedral void. The composition for $Co_{0.6}Fe_{0.8}GaMn_{2.6}ZnO_{8+\delta}$ (δ <<1) MCO is chosen in such a way so that an oxide solid solution evolves as CB-like microstructure consisting of distinct equilibrium phases, namely $CoFe_2O_4$, $CoMn_2O_4$, $ZnGa_2O_4$, and $ZnMn_2O_4$ or their possible combinations with mixed chemistry. Although a smaller grain size helps improving the storage density, it should not be achieved at the cost of its ferromagnetic properties. To develop a magnetic CB structure meeting with all the above-mentioned criteria, spinel structures are most

suitable due to their structural flexibility (only 33% of the interstitial space fills up by the cations) [5]. It is well reported that cationic site preference in the spinel structure (in $CoFe_2O_4$, of Co and Fe ions) is subjected to corresponding Gibbs free energy. Gibbs free energy of a material system is governed by various factors, e.g., size effect of constituent atoms, their coulomb interaction, and temperature-dependent entropy contribution. In a spinel system, physical properties such as magnetic behaviour, catalytical ability and ionic conductivity are dependent on the cationic distribution over interstitial sites. Spinel structures are classified based on the degree of inversion 'x', which signifies the ionic distribution of bivalent and trivalent cations at A and B sites in oxygen-based FCC framework. A spinel structures can be denoted as $(A_{1-x}B_x)_{Tet}(A_xB_{2-x})_{Oct}O_4$, where x = 0 and 1 denote normal spinel and inverse spinel structures, respectively [5]. In a normal spinel structure, tetrahedral and octahedral sites gets occupied by divalent and trivalent cations, respectively. On the other hand, in inverse spinels, octahedral sites gets solely occupied by divalent cations, while trivalent cations sit in the tetrahedral and octahedral sites evenly. Hence, it is possible to develop CB like microstructure with desired properties in a spinel system by putting appropriate elements together in a critical stoichiometric combination followed by a specific heat treatment. At lower temperatures, there will be a competition between the size effect and coulombic interaction of a cation with the surrounding oxygen atoms that decides the occupancy in an interstitial void [6]. For instance, in $CoFe_2O_4$, Fe^{+3} and Co^{+2} ions search for the appropriate void to occupy in order to attain maximum stability. In spinels, an octahedral sites in the influence of coulombic interaction (created with six surrounding oxygen ions) attract Fe^{+3} ion more strongly than Co^{+2} ion. On the other side, tetrahedral site (created with four oxygen atoms) also attract Fe^{+3} atom but with less intensity. Contrary to that, under the influence of size effect, a larger size of Co^{+2} ion (0.72 Å) compared to Fe^{+3} (0.64 Å) looks for a bigger interstitial octahedral site than that of the tetrahedral site (here the entropy contribution is negligible) [7]. Crystal field stabilisation theory (CFST) suggests the dominance of the size effect over the Coulomb effect because normal spinel is energetically higher than inverse spinel by 0.339 eV/Co. Moreover, the entropy term gets involved as the temperature increases. It remarkably influences the Co and Fe ions distribution and pushes A, B cationic species into two different sites in a spinel structure.

Here, we have engineered the parental $CoFe_2O_4$ and $ZnGa_2O_4$ spinel structures with elements such as Fe, Co, and Zn, Ga in the authority of Mn^{+3} ion. Among all, Fe, Co and Mn are J-T active elements with an increasing ability to introduce distortion in the crystal

structure. J-T distortion introduces a miscibility gap in the parent compound of J-T active and inactive J-T ions, which sets the track for chemical phase separation leading to form J-T active ion-rich and poor regions. In $Co_{0.6}Fe_{0.8}GaMn_{2.6}ZnO_{8+\delta}$ MCO, except Zn^{+2} and Ga^{+3} ions, all other participants are J-T active either in low spin or high spin electron filling conditions. Mn^{+3} and Co^{+2} have d^4 and d^7 orbitals that can degenerate in both the low and high spin filling. In high spin, the crystal field stabilization energy (CFSE) of Mn^{+3} and Co^{+2} are -6 Dq and 12 Dq, respectively, where Mn^{+3} introduces high J-T distortion in the system compared to Co^{+2} cations.

On the other hand, Mn^{+2} and Fe^{+3} ions [d^5] only become J-T active ions in the low spin filling. At the same time, Fe^{+2} and Co^{+3} [d^6] turn J-T active in a high spin filling configuration. Oxygen is a weak legend, which produces high spin electron filling configuration in the d-orbital. Hence, a cation that produces J-T distortion in high spin conditions will be considered J-T active. Although J-T distortion introduced by Fe^{+2} and Co^{+3} is weak, it will still affect crystal structure. The cumulative effect of orbital shapes and size of the constituent ions , and their interactions governs the final lattice parameters of the equilibrium phases. Any variation in the lattice parameter may introduce the distortion in structure this situation can lead to the phase transition.

In contrast to most metallic systems, ceramic manganite spinel systems, e.g., $CoFeMnO_4$, $Mg(ZnMn)O_4$ [1], and $ZnGaMnO_4$ [8] develop CB-like microstructure through pseudospinodal decomposition of the cubic solid solution [9]. The decomposition separates a cubic matrix into two cubic and tetragonal phases with Mn-rich and Mn-lean compositions. Ideally, the $CoFe_2O_4$ spinel structure possesses $Fd\bar{3}m$ space group, but after phase separation induced by J-T active Mn^{+3}-ion, another $CoMn_2O_4$ tetragonal phase with $I4_1/amd$ space group comes into the co-existence [3]. However, in both the metallic and ceramic systems, CB evolution is driven by a coherent strain (a consequence of thermodynamic or compositional fluctuations), which assembles two or more orientation variants of the ordered or compositionally separated phases in 3D. This 3D assemblage of the nanodomains helps a decrease in the microstructure's overall free energy by minimizing the lattice parameter misfit in their respective phases. The formation of the symmetry lifting phase is common in both the systems. The cooling rate is another critical parameter for CB microstructure evolution, second to stoichiometry, which governs interdependently the magnetic and electric properties. Cooling rate also controls the unit cell parameters [7]. In the case of rapid quenching, Mn^{+3} ions do not get a chance to occupy the octahedral void and could not be J-T active ions for a cooperative J-T distortion. Once the cooling rate

reduces sufficiently, Mn^{+3} can get sufficient time to diffuse to occupy the octahedral position (B site), where it becomes J-T active ion and introduces distortion (> 10%) to compensate for the electronic degeneracy. Magnetic properties of the entire microstructure depend on the arrangement of the nanodomains, and within the individual nanodomain how magnetic ions are arranged in the unit cell. In a unit cell, the magnitude and direction of their magnetic moments (cumulative spin and orbital) defines the overall magnetic moment of the cell. Since the positioning of the cations is subjected to the cooling rate also, there will always be a critical cooling rate for which desired magnetic properties in a CB microstructure with appropriate domain size can be achieved. Despite various investigations made so far in spinel manganites, CB-like microstructural evolution in MCO is a new exploration and deserves further elucidation.

6.2 Materials and methods

The CB-like microstructure in MCO samples were prepared by a solid-state synthesis route. All ultra-high pure precursor powders of Co_2O_3, ZnO, Mn_2O_3, Ga_2O_3, and Fe_2O_3 (Alfa Aesar and Sigma Aldrich) were mixed and palletised in four stoichiometric ratios: $Co_{0.6}Fe_{0.8}Mn_{1.6}O_4$, $ZnGaMnO_4$, $Co_{0.6}Fe_{0.8}GaMn^{+4}_{2.6}ZnO_{8+\delta}$ ($\delta<<1$) and $Co_{0.6}Fe_{0.8}Ga(Mn^{+3}_{1.6}+Mn^{+4}_{1})ZnO_{8+\delta}$ ($\delta<<1$). Since we have already established the parameters for optimum evolution of the CB-microstructure in $Co_{0.6}Fe_{0.8}Mn_{1.6}O_4$, a further addition of Zn and Ga into the CoFeMnO should result in the formation of a more complex CB-like microstructure. A study on the ZnGaO system was obligatory. For that purpose, $ZnGa_{2-x}Mn_xO_4$, x = 0.5, 1, and 1.6 samples were prepared, and for each value of x three pellets were made. All the pellets were sintered at 1250 ℃ for 24 hours and was brought down to room temperature through three different routes: annealing, quenching and a combination of quenching and ageing at 375℃ for 150 hours. All the MCO pellets were sintered in the air atmosphere at 1250 ℃ for 24 hours and then followed by ice water quenching. To increase the diffusion kinetics for cooperative movement of J-T active ions, an ageing treatment at 375 ℃ was given to the samples. To study the evolution process in continuation, sintered and quenched samples were aged for 25 hours, 100 hours, 150, and 250 hours. TEM samples were prepared by drop-casting of fine powders obtained from perfectly ground sintered pellets, onto the carbon-coated Cu grid. Tecnai G^2 T20 loaded with LaB_6 thermionic emission e-source was used for TEM investigations. All the XRD analysis for phase identification has been carried out on a Pananalytical HRXRD machine using Bragg-Brentano theta-theta geometry.

6.3 Results and discussion

To obtain CB-like microstructure in a MCO made of Co, Fe, Ga, Mn and Zn, it was obligatory to study the effect of Ga and Zn on its crystal structure. For that purpose, $ZnGa_xMn_{2-x}O_4$ samples were investigated with a well-planned set of experiments. These experiments are designed to study the various composition and heat treatment combinations. In this study, nine pellets of $ZnGa_xMn_{2-x}O_4$ with x = 0.5, 1, 1.6 were made through green sintering at 1250 °C for 24 hours, followed by cooling through three different routes in order to achieve a stable CB-like microstructure.

6.3.1 XRD analysis

Figure 6.1(a) shows XRD patterns of $ZnGa_xMn_{2-x}O_4$ samples with x=1 and sintered at 1250 °C for 24 hours, followed by cooling through three different routes. The first XRD pattern (black) corresponding to a sintered and annealed (slow cooled) $ZnGaMnO_4$ sample shows the presence of cubic and tetragonal phases with significant peak broadening and splitting. The second XRD pattern (red) corresponds to sintered and quenched $ZnGaMnO_4$ sample. In this pattern, all the peaks are matching to a cubic spinel phase with $Fd\bar{3}m$ space group. However, little shouldering at the bases of all peaks that signifies the presence of a tetragonal phase in a minute fraction. In the same figure, XRD pattern (blue) corresponds to $ZnGaMnO_4$ sample solutionized at 1250 °C for 24 hours, followed by quenching and ageing at 375 °C for 75 hours. This XRD pattern illustrates the presence of cubic and tetragonal phases with a clear split in the peaks.

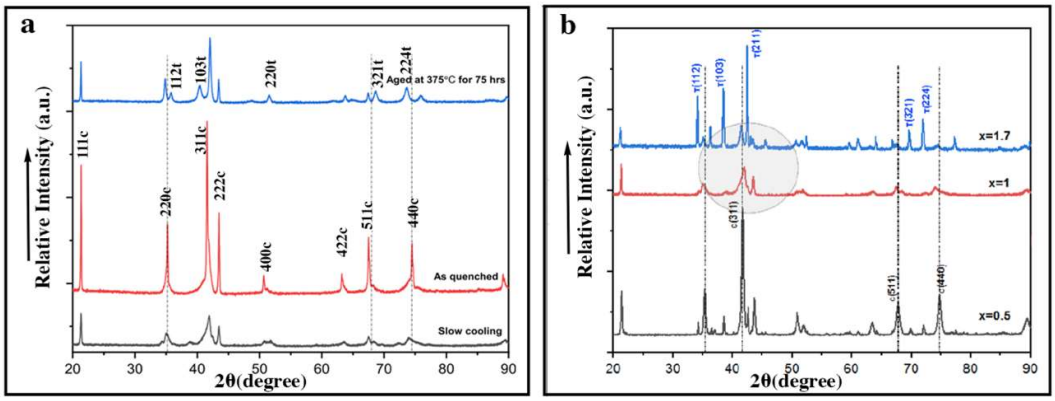

Figure 6.1: *XRD patterns for $ZnGaMnO_4$ (a) heat treatment establishment (b) stoichiometry establishment.*

The peaks match with cubic and tetragonal phases with $Fd\bar{3}m$ and $I4_1/amd$ space groups, respectively. In Figure 6.1(b) a critical observation of all the XRD peaks suggests that $ZnGa_xMn_{2-x}O_4$ sample with x = 1 exhibits equal intensities of cubic and tetragonal peaks [8]. The comparable intensities of both the phases signify the presence of cubic and tetragonal domains with almost equal volume, which makes $ZnGa_xMn_{2-x}O_4$ sample with x = 1 most suitable for CB-formation. Hence the cumulative choice of x = 1 and sintering at 1250 ℃ for 24 hours and ageing at 375 ℃ for 75 hours is the appropriate stoichiometry and heat treatment to obtain an optimum CB-like microstructural evolution in $ZnGaMnO_4$. With this reasoning, it is established that for both Mn-doped $CoFe_2O_4$ and $ZnGa_2O_4$ spinel manganites, a particular stoichiometry (with a tendency to decompose in equal volume of cubic and tetragonal phases) with a fixed heat treatment (sintering at 1250 ℃ for 24 hours followed by quenching and ageing at 375 ℃ for long hours) is a suitable combination to obtain a CB-like microstructure.

A Co, Fe, Mn, Zn, Ga-based MCO has been developed and characterized for this study. Further MCO samples were used for characterization with TEM diffraction contrast imaging to excite various CB-like microstructural features to understand its constituent phases and its morphological distribution. Figure 6.2 illustrates the stacks of XRD patterns of $ZnGaMnO_4$, $Co_{0.6}Fe_{0.8}Mn_{1.6}O_{4+\delta}$, $Co_{0.6}Fe_{0.8}GaMn^{+4}_{2.6}ZnO_{8+\delta}$, $Co_{0.6}Fe_{0.8}Ga(Mn^{+3}_{1.6}+Mn^{+4}_{1})ZnO_{8+\delta}$, $\delta<<1$, in two different heat treat treatment conditions for comparative study. Figure 6.2(a) shows stack of XRD pattern after sintering and quenching. In as quench condition, all the samples match with a cubic spinel phase with $Fd\bar{3}m$ space group. Whereas Figure 6.2(b) shows a stack of sintered-quenched and aged samples for 150 hours. In this figure, all the XRD patterns except $Co_{0.6}Fe_{0.8}GaMn^{+4}_{2.6}ZnO_{8+\delta}$ sample, show a clear peak split in all of the major peaks, the split peaks match with cubic ($Fd\bar{3}m$) and tetragonal ($I4_1/amd$) spinel phases (denoted by subscript of indices). This alienated behaviour of $Co_{0.6}Fe_{0.8}GaMn^{+4}_{2.6}ZnO_{8+\delta}$ can be referred to as the absence of J-T distortion because this sample contains Mn^{+4} ion instead of Mn^{+3} ion, which does not show degeneracy of d-orbital. XRD results in Figure 6.2 (b) suggest that $Co_{0.6}Fe_{0.8}Ga(Mn^{+3}_{1.6}+Mn^{+4}_{1})ZnO_{8+\delta}$ sample is promising for CB-like microstructural evolution. Henceforth, for further analysis, this sample is chosen for study.

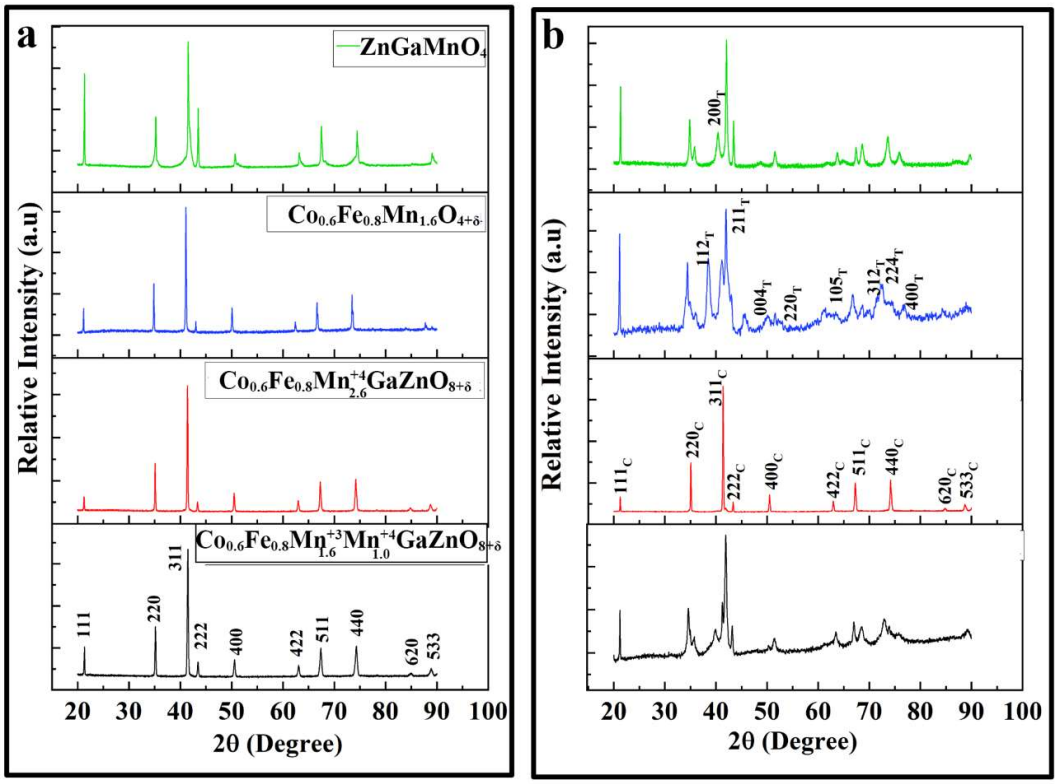

Figure 6.2: *XRD patterns of $ZnGaMnO_4$, $Co_{0.6}Fe_{0.8}Mn_{1.6}O_{4+\delta}$, $Co_{0.6}Fe_{0.8}GaMn^{+4}_{1.6}ZnO_{8+\delta}$, and $Co_{0.6}Fe_{0.8}Ga(Mn^{+3}_{1.6}+Mn^{+4}_{1})ZnO_{8+\delta}$, where $\delta<<1$ (a) sintered at 1250 ℃ for 24 hours followed by quenching in ice water (b) sintered at 1250 ℃ for 24 hours followed by quenching in ice water and aged at 375 ℃ for 150 hours.*

6.3.2 Diffraction contrast microscopy

When $Co_{0.6}Fe_{0.8}Ga(Mn^{+3}_{1.6}+Mn^{+4}_{1})ZnO_{8+\delta}$, $\delta<<1$ sample was looked at from different Zone axes, its appearance changed from the stripe to brick wall to CB (Figure 6.3). All these appearances are the consequence of the well-defined mutual orientation of the nanodomains in a 3D space. A systematic excitement at specific tilt conditions excites various microstructural features, i.e., domain boundaries, facets, and subdomains that gives an intriguing appearance to the microstructure. In this study, diffraction contrast tilt investigation at various steps of the evolution is utilized to reconstruct the microstructure in 3D.

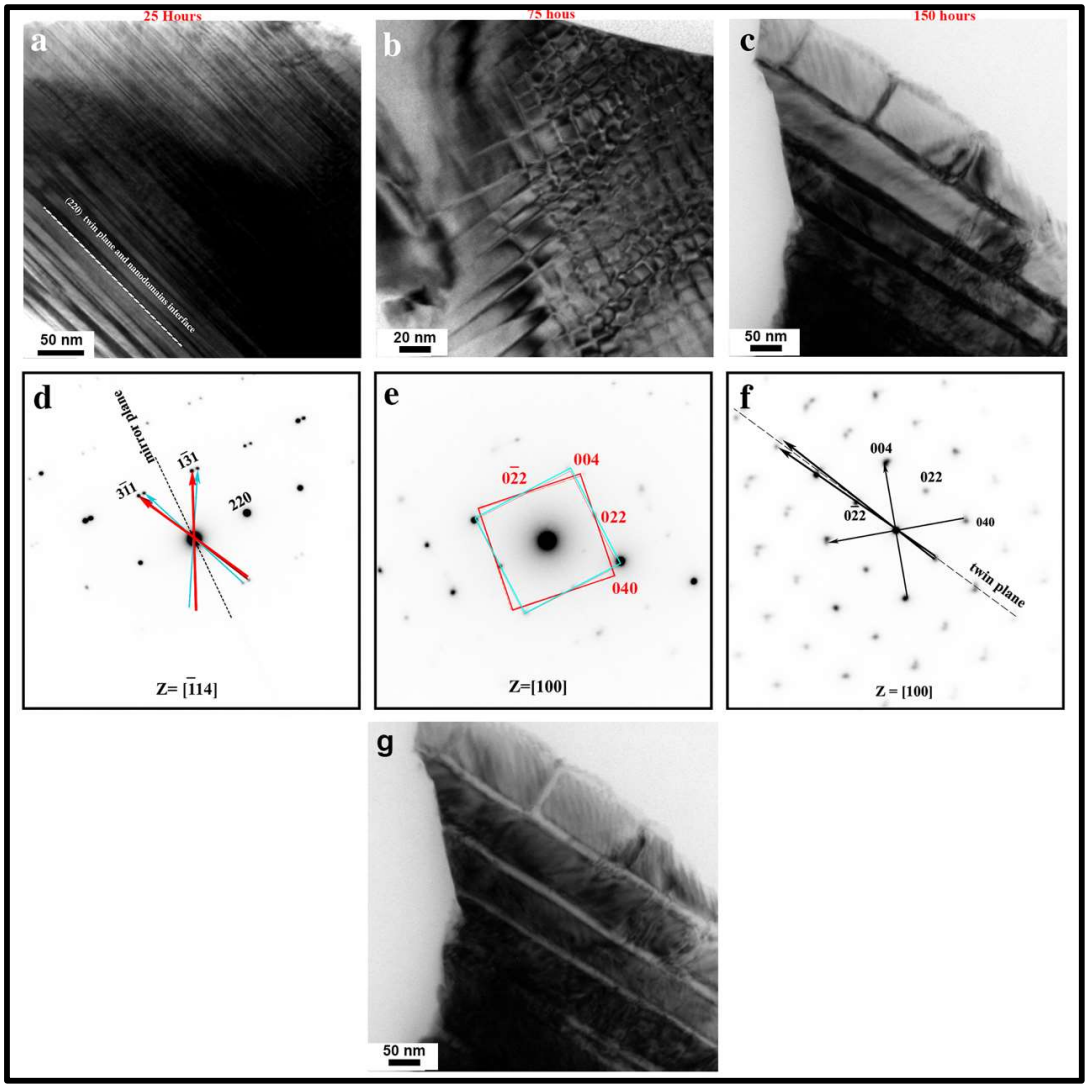

Figure 6.3: *Bright field image and corresponding electron diffraction pattern of* $Co_{0.6}Fe_{0.8}Ga(Mn_{1.6}^{+3}+Mn_{1}^{+4})ZnO_{8+\delta}$ *sample sintered at 1250 ℃ for 24 hours and quenched into ice water followed by ageing at 375 ℃ for (a) 25 hour (b) 75 hours (c) 150 hours. Here different type of zone axes (two fold and four fold) were taken to visualized different appearance of the microstructure (g) dark field image corresponding to (c) considering 022 spot.*

These tilt experiments were performed on $Co_{0.6}Fe_{0.8}Ga(Mn_{1.6}^{+3}+Mn_{1}^{+4})ZnO_{8+\delta}$ samples, prepared with interrupted heat treatment. To make samples for such investigation, four samples of $Co_{0.6}Fe_{0.8}Ga(Mn_{1.6}^{+3}+Mn_{1}^{+4})ZnO_{8+\delta}$ were sintered at 1250 ℃ for 24 hours, followed by ageing at 375 ℃ for 25 hours, 100 hours, 150 hours and 250 hours.

Figure 6.3(a) shows a bright-field image of the sintered and aged (25 hours) $Co_{0.6}Fe_{0.8}Ga(Mn_{1.6}^{+3}+Mn_{1}^{+4})ZnO_{8+\delta}$ sample along $[1\bar{1}4]$ zone axis. This figure reveals a strip-like appearance of the CB-like microstructure. This strip-like appearance of the microstructure originates from alternative bright and dark nanorods with a half wavelength of ~10 nm. Corresponding electron diffraction pattern (figure 6.3(d)) taken from the centre of the Figure 6.3(a) confirms the presence of two twinned orientation variants of a tetragonal phase in the microstructure. These tetragonal orientation variants are twinned along (022) planes. The same microstructure changes its appearance when looked at from the [100] zone axis. This CB-like appearance, with square domains (~15 nm X ~15 nm), is shown in Figure 6.3(b), taken from the same sample after ageing for 75 hours. The corresponding electron diffraction pattern (Figure 6.3(e)) confirms that these nanodomains share perpendicular interfaces along (022) and $(0\bar{2}2)$ planes. In the same diffraction pattern, another set of similar 004 types of spots, split with 7.4° in-plane rotation concerning the previous set, suggesting the presence of two orientation variants of the cubic phase in the microstructure. When a similar tilt experiment was performed for 150 hours aged $Co_{0.6}Fe_{0.8}Ga(Mn_{1.6}^{+3}+Mn_{1}^{+4})ZnO_{8+\delta}$ sample along [100] zone axis, a brick-wall-like appearance of the microstructure was obtained (Figure 6.3(c)). This intriguing brick-wall-like appearance shows significantly large rectangular domains (150 nm X 450 nm) with thick boundaries along (022) and $(0\bar{2}2)$. To further investigate the broadening of the domain boundaries, a dark field image is taken by selecting 022 kinds of spots (Figure 6.3 (g), which shows a reversal of contrast with very sharp bright domain boundaries with significant broadening. This dark field observation points out two possibilities for such an intriguing phenomenon, first suggests the presence of another domain with incomplete evolution due to the sluggish diffusion of some cations. The second possibility recommends the presence of similar domains that are gone out of the Bragg diffraction condition due to their mutual orientation.

Figure 6.4(a) shows similar thick domain boundaries in a 150 hours aged sample. When looking from $[1\bar{1}\bar{1}]$ zone axis, the same sample depicts alternative 100 nm wide stripes with a 022 plane as the twinned interface (Figure 6.4(b)). Each alternative stripe contains CB-like square domains of 7 nm X 7 nm with an interface subtending 45° with the parental twinned interface (marked with arrows). However, there are traces of similar nanodomains in the alternative stripe that is not showing CB-like subdomains.

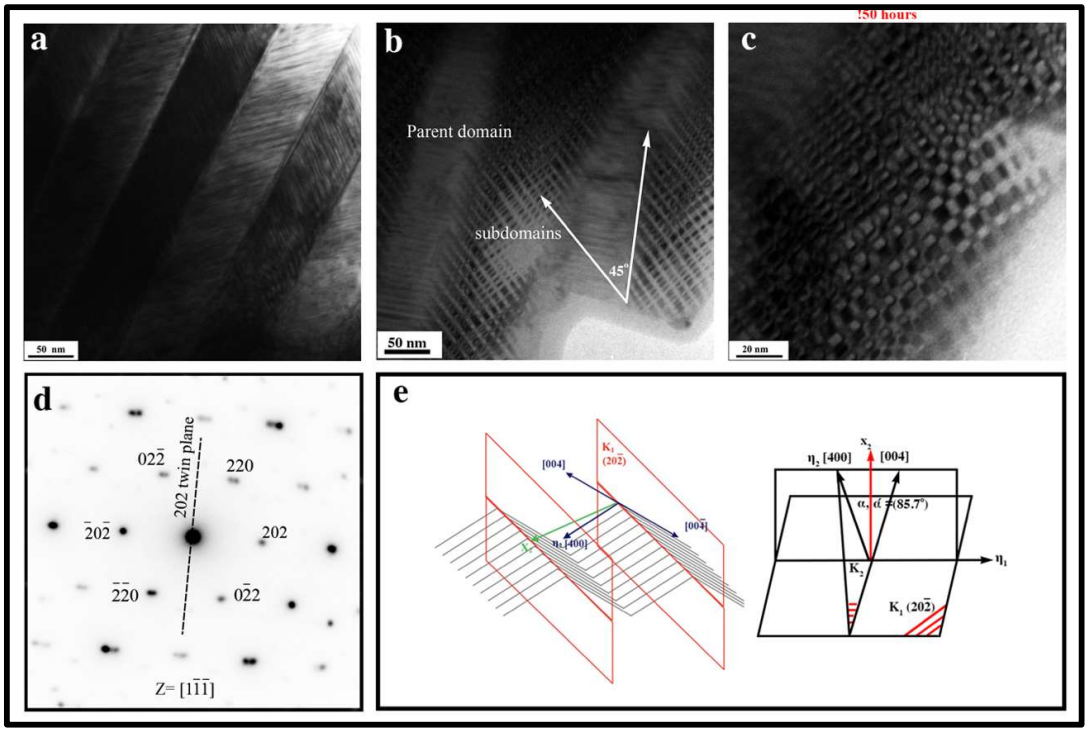

Figure 6.4: *Bright field image of* $Co_{0.6}Fe_{0.8}Ga(Mn_{1.6}^{+3}+Mn_{1}^{+4})ZnO_{8+\delta}$ *after sintering at 1250 °C and aging at 375 °C for 150 hour (a) herringbone-like appearance of microstructure, here strip-like domains are sharing thick interface (b) CB-like appearance of same microstructure and (d) corresponding electron diffraction pattern along* $[1\bar{1}\bar{1}]$ *zone axis showing twinning in (202) planes.(c) magnified view of one domain in (b). (e) schematic representation of all the twinning elements involved.*

The zoomed in version of a stripe from figure 6.4 (b) depicts CB-like appearance of the microstructure consisting of square and rectangular domains. A critical observation of these subdomains shows that there are two different shapes of dark domains patterned diagonally. Whereas bright domains are in single shape patterned perpendicularly. The Bright field image shown in figure 6.4 (b) and corresponding electron diffraction pattern shown in figure 6.4 (d) exhibit a twin relationship between the parental stipe-like domains. Figure 6.4 (e) depict a schematic representing K_1 $(20\bar{2})$ type plane as composition plane (or twin plane), η_1 and η_2 are the shear directions and x_2 (rotation axis) is the perpendicular to K_1 that bisects η_2 and η_2'. Here η_1 is contained in K_1 plane [10]. To address these irregularities (thick domain boundary and inconsistent shape of subdomains) in the microstructure, same sample was aged for 250 hours and was investigated with a tilt experiment in diffraction

contrast mode. Figure 6.5 shows BF images and corresponding electron diffraction patterns of sintered and 250 hours aged $Co_{0.6}Fe_{0.8}Ga(Mn^{+3}_{1.6}+Mn^{+4}_{1})ZnO_{8+\delta}$ sample. Bright-field image along [$2\bar{3}3$] zone axis is shown in figure 6.5(a), which exhibits similar thick domain boundaries (marked with a dotted line). The magnified view of similar feature is given in Figure 6.5 (d). Figure 6.5 (e) shows the corresponding electron diffraction pattern from the region given in Figure 6.5 (a), exhibiting two sets of diffraction spots twinned on ($0\bar{2}2$) planes. The particle in Figure 6.5 (a) was tilted from α = 20.1° to 4.86°, with a minute tilt in β used to correct image quality by bringing the particle precisely edge-on. However, the sample did not change its appearance significantly further ~ 15.5° in the counter-clockwise or negative α direction (Figure 6.5(a-c)). At α ~ 4.86° (Figure 6.5a), the binary stripe-like contrast with a thick interface is observed which is changed to four different contrast (marked as 1, 2, 3 and 4) with the sharp interface (Figure 6.5(b)). These domains with four different contrast (marked as 1, 2, 3 and 4) sharing a twinned interface on ($02\bar{2}$) plane as observed from the diffraction pattern in figure 6.5(f). A critical observation of figure 6.5(b) endorses that the contrast and width of every nanorod and the nature of their interfaces are different. Nanorods 1, 2, 3, and 4 are 25 nm, 21 nm,15 nm and 18 nm wide, respectively. Stripe 1 is darkest and broadest, whereas stripes 2 and 4 are bright and moderate in width. Contrary to all, stripe 3 is narrower and shows an exotic contrast at both the (022) interfaces. Figure 6.5(c) shows the edge-on view of all these interfaces. The interface between 1 and 2 rods is straight and well defined. On the other hand, the interface between 2-3 and 3-4 is hazy and unclear. This difference in the width of the nanodomains is also visualised in Figure 6.4(c). Where the size of rectangular domains is not equal, there are two different types of dark domains with similar-sized bright domains. Due to the nanodomain's mutual orientation, a precise systematic tilting along the appropriate zone axis excites various microstructural features in them. These orientations are in both in-plane and out of the plane directions. When one domain comes closer to the Bragg's diffraction condition, another will have to digress, and the contribution of diffracted intensity in the transmitted beam from both the domains would be different. Consequently, in the diffraction contrast mode, some of them have shown an intriguing opposite contrast. The domain closer to the diffraction condition will appear dark and vice-versa.

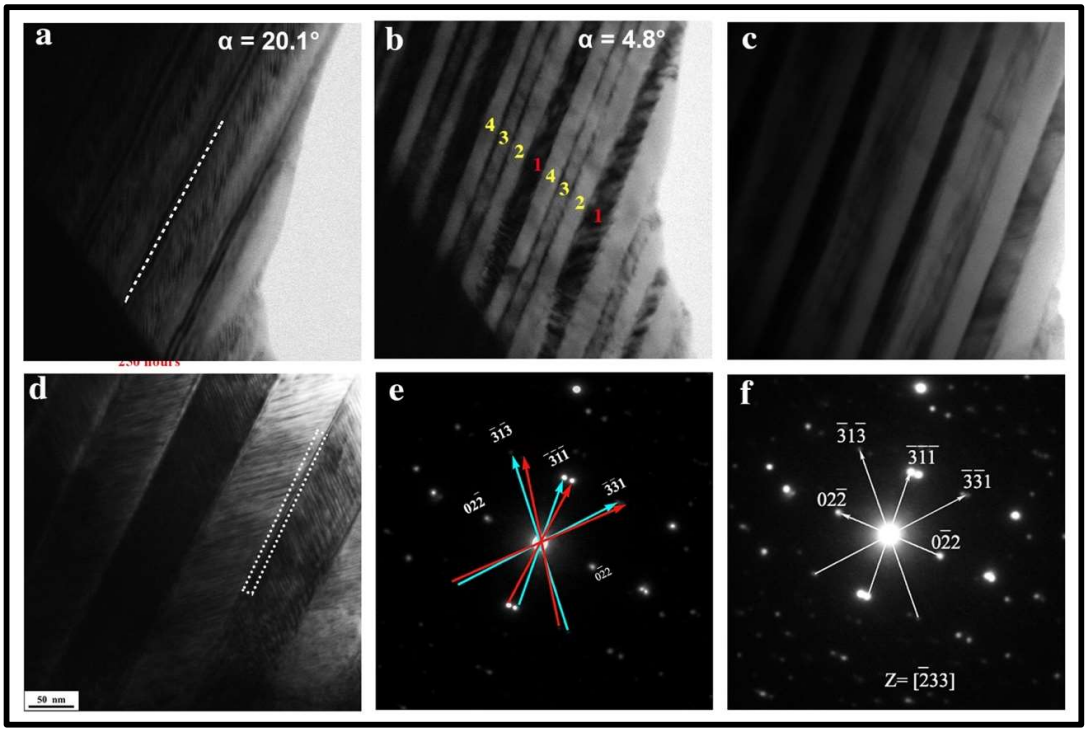

Figure 6.5 *(a-d) Bright field diffraction contrast images along* [$\bar{2}$33] *zone axis illustrating strip-like appearance CB-like microstructure at various tilt conditions at (a) α = 20.1° it resembles a layered interface, (b) α = 4.8° it shows alternative strips with four different contrasts (marked by numbers) representing an intriguing microstructure with domains of different mutual orientation and width. (c) an edge-on view of (b). (e) corresponding electron diffraction pattern for (b). (f) electron diffraction pattern for edge-on view shown in (c).*

A comparative analysis of all the bright-field images of the $Co_{0.6}Fe_{0.8}Ga(Mn_{1.6}^{+3}+Mn_{1}^{+4})ZnO_{8+\delta}$ sample sintered at 1250 °C for 24 hours followed by ageing at 375 °C for 25 hours, 75 hours, and 150 hours shown in figure 6.3 (a-c), suggests that the size of nanodomains increases with ageing time. Corresponding electron diffraction patterns along with various zone axis exhibit that irrespective of their appearance in the microstructure (stripe, brick-wall or CB-like), all the interfaces are 022 types of twinned interface. Figure 2(a,e) shows a bright field and corresponding diffraction pattern of a $Co_{0.6}Fe_{0.8}Ga(Mn_{1.6}^{+3}+Mn_{1}^{+4})ZnO_{8+\delta}$ sintered, quenched and aged for 25 hours sample showing a stripe-like microstructure consisting of tetragonal phase with two orientation variants twinned on (022) plane.

On the other hand, figures 6.2(b,f) depict the bright-field image and corresponding diffraction pattern of $Co_{0.6}Fe_{0.8}Ga(Mn_{1.6}^{+3}+Mn_{1}^{+4})ZnO_{8+\delta}$ sample after sintering and quenched followed by 75 hours ageing. Bright field image shows a CB appearance of microstructure with 15 nm X 15 nm square nanodomains sharing 022 and $(0\bar{2}2)$ planes as interface. The corresponding diffraction pattern shows two sets of four-fold diffraction patterns that are 4.5° mutually rotated, referring to the presence of a cubic domain with the two-phase variant. Figure 6.2 (c, d) shows the bright-field image and corresponding diffraction pattern of $Co_{0.6}Fe_{0.8}Ga(Mn_{1.6}^{+3}+Mn_{1}^{+4})ZnO_{8+\delta}$ sample sintered, quenched and aged for 150 hours. Rectangular nanodomains with 75 nm X 150 nm are visible in the bright field image, separated by significantly thick domain boundaries along 022 and $(0\bar{2}2)$ planes. This thick and dark contrast of the domain boundary could result from strain field, compositional segregation or a secondary phase in the microstructure. Since the sample was subjected to prolonged ageing treatment at 375 °C, the possibility of a strain field can be simply ruled out. To investigate two other possibilities same feature was looked at in dark field mode by selecting the 022 spots. Obtained dark field is shown in figure 6.2(d), which shows a reversal of contrast in the whole sample, and very sharp, bright and uniform contrast discards any random segregation of cations at domain boundaries. A critical observation of the same sample has been done to probe the matter further, providing us with some more interesting appearances of the CB microstructure. The Bright field image and corresponding electron diffraction pattern along [111] show a well-organised chessboard like square nanodomains in the alternative thick strips with an exotic alternative contrast (figure 6.3 (a, b)). These parent and product phases are oriented in such a manner so that they may minimise both interfacial and strain energies, in turn minimising the total free energy of the whole system. There is also a contribution of magnetic and electric field energy attached to the cubic and tetragonal nanodomains in the organisation of well-arranged properties, which influence the lattice parameters of corresponding cells. The lattice misfit of both the nanodomains defines the mutual orientation of the adjacent nanodomains. Approximately ~4.5° in-plane rotation in the twinned nanodomains has been observed in every spinel system. This can be clearly seen in the twinned electron diffraction patterns (Figure 6.1(d), 6.2(b), 6.3(d)). The misfit in lattice parameters relates the domain wall angles with a relationship. Ideally, $CoFe_2O_4$ acquires a cubic ferromagnetic phase with a~8.3 Å at Tc~800 K, and $CoMn_2O_4$ adopt a tetragonal paramagnetic phase with a~8.2 Å, c~9.3 Å at Tc~100 K. In the presented CB microstructure these phases have not separated

in the pure forms. Instead, a cubic matrix decomposes in one tetragonal phase with two orientation variants with a~8.0 Å and c~8.7 Å and one cubic phase with two-phase variants a~8.3 Å. The critical factor responsible for the chessboard-like microstructure formation is the crystallography of the phase transformation. The optimum balance between strain energy and surface energy is a key factor in the formation and evolution of coherent microstructures.

The oxidation states of the constituent elements in $CoFeGaMnZnO_{8+\delta}$ sample sintered at 1250 °C for 24 hours followed by ageing at 375 °C for 150 hours were observed by X-ray photoelectron spectroscopy (XPS). XPS graphs shown in Figure 1 (a, b) confirm that Co is majorly present in Co^{+2} oxidation state, while Fe is present in Fe^{+2} and Fe^{+3} oxidation states. Figure 1c exhibits that Mn is present in two major oxidation states Mn^{+3} and Mn^{+4}. Figures 1(d-f) confirms the presence of Ga and Zn majorly in Ga^{+3} and Zn^{+2} oxidation states, respectively.

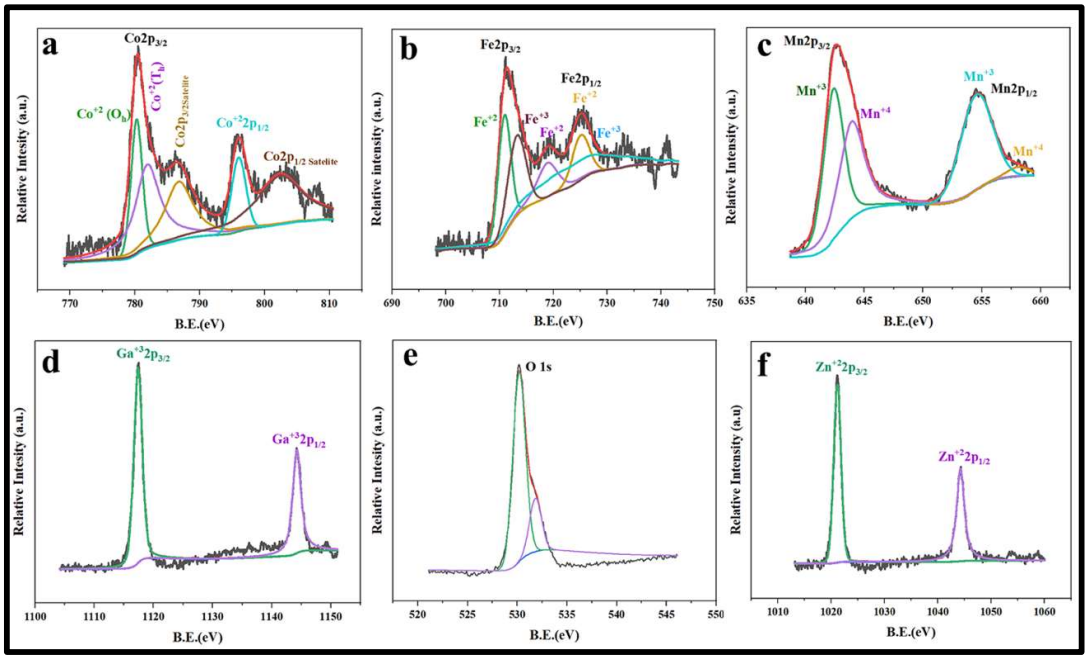

Figure 6.6: *The X-ray Photoelectron spectroscopy (XPS) graphs of $CoFeGaMnZnO_{8+\delta}$ are showing oxidation sates of constituent elements (a) Co (b) Fe (c) Mn (d) Ga (e) O (f) Zn.*

6.4 Conclusions

The similarities between the CB-like microstructural features obtained in MCO CoFeGaMnZnO spinel system, and CoFeMnO and ZnGaMnO ternary systems corroborate the thought that the mechanism of CB-like microstructural evolution is crystal structure-

dependent. In all the manganite systems mentioned above, the evolution of cuboidal and stripe-like nanodomains sharing interfaces in {022} planes happens with a series of phase transformation events. However, in contrast to CoFeMnO and ZnGaMnO ternary systems, the evolution of CB-like microstructure in MCO is more complex. The presence of nanodomains with more than two types of contrast and size concludes the existence of a more complex microstructure. The juxtaposition of XRD patterns corresponding to $Co_{0.6}Fe_{0.8}Ga(Mn^{+3}_{1.6}+Mn^{+4}_{1})ZnO_{8+\delta}$ and $Co_{0.6}Fe_{0.8}Ga(Mn^{+3}_{2.6})ZnO_{8+\delta}$ after appropriate heat treatment confirms the role of J-T distortion as a main driving force in the evolution process. At the latter stage pseudospinodal decomposition may distribute the strain into different J-T active and J-T inactive phases, similar to the ternary phase (explained in Chapter 3 and Chapter 4).

The doping of Mn^{+3} ions disturbed the uniformity of the unit cells. It introduced the tetragonality due to its exotic splitting of d-orbital and resulting J-T distortion in e_g levels which triggers the phase separation process and divides the parent cubic system into a well-organised self-assembled nanodomain. This self-assembly is the essential feature by which the cubic parent phase has turned into twin-related metastable tetragonal phases with a minimal c/a ratio embedded into the cubic parent phase. Further decomposition of these metastable tetragonal domains into cubic and tetragonal phases gives birth to a CB-like structure. Henceforth, the chessboard system has coherent twinned interfaces between the structurally distinct nanodomains, which are compositionally distinguishable as well. To attain a stable phase configuration and a further reduction in total free energy of the whole system, gradual phase separation by spinodal decomposition has happened as the final stage of CB microstructural evolution.

References

[1] C.L. Zhang, S. Yeo, Y. Horibe, Y.J. Choi, S. Guha, M. Croft, S.W. Cheong, S. Mori, Coercivity and nanostructure in magnetic spinel $Mg(Mn,Fe)_2O_4$, Appl. Phys. Lett. 90 (2007) 133123. https://doi.org/10.1063/1.2717568.

[2] F.C. Gaspare Varvaro, Ultra-High-Density Magnetic Recording, Jenny Stanford Publishing, 2016. https://doi.org/10.1201/b20044.

[3] C.L. Zhang, C.M. Tseng, C.H. Chen, S. Yeo, Y.J. Choi, S.W. Cheong, Magnetic nanocheckerboards with tunable sizes in the Mn-doped $CoFe_2O_4$ spinel, Appl. Phys. Lett. 91 (2007) 233110. https://doi.org/10.1063/1.2821838.

[4] A.S. Pal, A.K. Lal Das, A. Singh, K.M. Knowles, M.I. Ahmad, J. Basu, Evolution of a self-assembled chessboard nanostructure spinel in a CoFeGaMnZn multicomponent oxide, Philos. Mag. 102 (2022) 1121–1135. https://doi.org/10.1080/14786435.2022.2035444.

[5] G. Pilania, V. Kocevski, J.A. Valdez, C.R. Kreller, B.P. Uberuaga, Prediction of structure and cation ordering in an ordered normal-inverse double spinel, Commun. Mater. 1 (2020) 84. https://doi.org/10.1038/s43246-020-00082-2.

[6] N. Li, X. Duan, F. Yu, H. Jiang, Effects of preparation method and temperature on the cation distribution of $ZnGa_2O_4$ spinel studied by X-ray photoelectron spectroscopy, Vacuum. 142 (2017) 1–4. https://doi.org/10.1016/j.vacuum.2017.04.035.

[7] Y.H. Hou, Y.J. Zhao, Z.W. Liu, H.Y. Yu, X.C. Zhong, W.Q. Qiu, D.C. Zeng, L.S. Wen, Structural, electronic and magnetic properties of partially inverse spinel $CoFe_2O_4$: a first-principles study, J. Phys. D. Appl. Phys. 43 (2010) 445003. https://doi.org/10.1088/0022-3727/43/44/445003.

[8] A. Kosuga, K. Kurosaki, K. Yubuta, A. Charoenphakdee, S. Yamanaka, R. Funahashi, Solid-state self-assembly of nanostructured oxide as a candidate high-performance thermoelectric material, J. Electron. Mater. 38 (2009) 1303–1308. https://doi.org/10.1007/s11664-009-0716-4.

[9] S. Yeo, S. Guha, S.-W. Cheong, Generic properties of Mn spinels with an immiscibility induced by a Jahn–Teller distortion, J. Phys. Condens. Matter. 21 (2009) 125402. https://doi.org/10.1088/0953-8984/21/12/125402.

[10] J.N. Reimers, J.R. Dahn, Electrochemical and in situ X-ray diffraction studies of lithium intercalation in $LixCoO_2$, J. Electrochem. Soc. 139 (1992) 2091–2097.

https://doi.org/10.1149/1.2221184.